Published in final edited form as:
Biomaterials. 2011 May ; 32(14): 3654–3665. doi:10.1016/j.biomaterials.2011.01.068.

Neuronal uptake and intracellular superoxide scavenging of a fullerene (C_{60})-poly(2-oxazoline)s nanoformulation

Jing Tong[a,b], **Matthew C. Zimmerman**[a,c], **Shumin Li**[c], **Xiang Yi**[a,b], **Robert Luxenhofer**[d], **Rainer Jordan**[d], and **Alexander V. Kabanov**[a,b,e,*]

[a] Center for Drug Delivery and Nanomedicine, University of Nebraska Medical Center (UNMC), Omaha, NE 68198, USA

[b] Department of Pharmaceutical Sciences, University of Nebraska Medical Center (UNMC), Omaha, NE 68198, USA

[c] Department of Cellular and Integrative Physiology, University of Nebraska Medical Center (UNMC), Omaha, NE 68198, USA

[d] Department Chemie, Technische Universität Dresden, 01062 Dresden, Germany

[e] Faculty of Chemistry, M.V. Lomonosov Moscow State University, 119899 Moscow, Russia

Abstract

Fullerene, the third allotrope of carbon, has been referred to as a “radical sponge” because of its powerful radical scavenging activities. However, the hydrophobicity and toxicity associated with fullerene limits its application as a therapeutic antioxidant. In the present study, we sought to overcome these limitations by generating water-soluble nanoformulations of fullerene (C_{60}). Fullerene (C_{60}) was formulated with poly(N-vinyl pyrrolidine) (PVP) or poly(2-alkyl-2-oxazoline)s (POx) homopolymer and random copolymer to form nano-complexes. These C_{60}-polymer complexes were characterized by UV–vis spectroscopy, infrared spectroscopy (IR), dynamic light scattering (DLS), atomic force microscopy (AFM) and transmission electron microscopy (TEM). Cellular uptake and intracellular distribution of the selected formulations in catecholaminergic (CATH.a) neurons were examined by UV–vis spectroscopy, immunofluorescence and immunogold labeling. Electron paramagnetic resonance (EPR) spectroscopy was used to determine the ability of these C_{60}-polymer complexes to scavenge superoxide. Their cytotoxicity was evaluated in three different cell lines. C_{60}-POx and C_{60}-PVP complexes exhibited similar physicochemical properties and antioxidant activities. C_{60}-poly(2-ethyl-2-oxazoline) (PEtOx) complex, but not C_{60}-PVP complex, were efficiently taken up by CATH.a neurons and attenuated the increase in intra-neuronal superoxide induced by angiotensin II (Ang II) stimulation. These results show that C_{60}-POx complexes are non-toxic, neuronal cell permeable, superoxide scavenging antioxidants that might be promising candidates for the treatment of brain-related diseases associated with increased levels of superoxide.

Keywords

Fullerene (C_{60}); Polyoxazoline; Antioxidant; Free radical; Neural cell

*Corresponding author. Center for Drug Delivery and Nanomedicine, 985830 Nebraska Medical Center, Omaha, NE 68198-5830, USA. Tel.: +1 402 559 9364; fax: +1 402 559 9365, akabanov@unmc.edu (A.V. Kabanov).

1. Introduction

The unique physical and chemical properties of fullerene (C_{60}) have elicited broad research interest from different areas since it was discovered in 1985 [1,2]. Over the past 20 years, fullerene has been investigated as a radical scavenger, due to its highly unsaturated structure and excellent electron-receptor properties [3–7]. It has been reported that one fullerene molecule can readily react with at least 15 benzyl radicals or 34 methyl radicals to form stable radical or non-radical adducts [4]. Many detrimental biological free radicals, such as superoxide ($O_2^{\bullet -}$), hydroxyl radical (OH), singlet oxygen ($^1O_2$) and nitrogen-based radicals can be efficiently scavenged by fullerene and fullerene derivatives [8–12]. However, the extreme hydrophobicity and potential toxicity of fullerene limit its application as a therapeutic antioxidant [7]. To overcome these barriers, two major categories of strategies have been developed in the last two decades: (1) Synthesis of water-soluble fullerene derivatives which maintain the radical scavenging capability, such as carboxyfullerene (C3) [11,13] and poly hydroxyfullerene (fullerenol) [11,14]; (2) Solubilization of pristine fullerene using polymer, surfactant, cyclodextrin, liposome, solvent exchange or nanomilling [9,15–21]. For example, a carboxylated fullerene derivative (C_{60} tris-malonic acid) was reported to be able to protect neurons from apoptosis induced by glutamate receptor-mediated excitotoxicity, and is now being commercially developed as a therapy for neurodegenerative diseases [11,22,23]. Several pristine fullerene formulations, such as fullerene-poly (N-vinyl pyrrolidine) (PVP) complex (Radical Sponge®) or fullerene-containing vegetable squalane (LipoFullerene®), have been approved as the antioxidant ingredients in cosmetic products and are sold in some countries [21,24–26].

Elevated levels of reactive oxygen species (ROS), including superoxide, hydroxyl radical, and hydrogen peroxide (H_2O_2) have been associated with the pathogenesis of numerous diseases, such as hypertension, heart failure, arthritis, cancer, and multiple neurodegenerative disorders [27–30]. More specifically, considerable evidence has shown that the intracellular signaling pathway of angiotensin II (Ang II), a vasoconstrictor peptide that increases sympathetic nerve activity causing an elevation of blood pressure, involves an increase in superoxide. In neurons, the Ang II-induced increase in superoxide modulates ion channel activity and increases neuronal excitations which are linked to neuro-cardiovascular diseases like hypertension and heart failure [31–35]. Therefore, it is believed that scavenging superoxide in the central nervous system (CNS) is a rational strategy for the treatment of Ang II-dependent cardiovascular diseases.

It is well known that fullerene, as an electron-receptor, can be solubilized by polymers containing electron-donors (like amide groups) to form water-soluble charge-transfer complexes [17]. These fullerene–polymer complexes, of which C_{60}-PVP has been the most widely studied, usually have high aqueous solubility, high colloidal stability, narrow size distribution and low toxicity, which are suitable for biological and pharmaceutical applications [17,24]. In the present study, we report that another type of biocompatible polymers, poly(2-alkyl-2-oxazoline)s (POx), can also form water-soluble, antioxidant–active complexes with fullerene. One type of C_{60}-PVP (PVP 10 kDa) and two types of C_{60}-POx (PEtOx 5 kDa, and P (EtOx-*co*-BuOx) 8 kDa) complexes were prepared and their physicochemical properties and superoxide scavenging activities were quantitatively measured and compared. Based on these results, the optimal formulations were further investigated as intracellular superoxide scavengers in cultured neurons stimulated with Ang II. Their cellular uptake and distribution were also studied using various techniques.

2. Materials and methods

2.1. Materials

Fullerene (C_{60}), PVP 10 kDa (K15), toluene, chloroform, hypoxanthine (HX), xanthine oxidase (XO), angiotensin II (Ang II), riboflavin 5′-monophosphate sodium salt dehydrate (FMN) and superoxide dismutase (SOD1) were purchased from Sigma–Aldrich Co. (St-Louis, MO). Poly(2-ethyl-2-oxazoline) 5 kDa (PEtOx) was purchased from Polysciences Inc. (Warrington, PA). Poly(2-ethyl-2-oxazoline)-*co*-poly (2-butyl-2-oxazoline) 8 kDa ($P(EtOx_{50}$-*co*-$BuOx_{20})$) was synthesized and purified as described before [36]. Methoxycarbonyl-2,2,5,5-tetramethyl-pyrrolidine (CMH), deferoxamine methanesulfonate salt (DF) and diethyldithiocarbamic acid sodium (DETC) were from Noxygen Science Transfer & Diagnostics GmbH (Elzach, Germany). Fullerene monoclonal antibody (mouse IgG1) was purchased from Santa Cruz Biotechnology, Inc. (Santa Cruz, CA). Alexa Fluor® 488 goat anti-mouse IgG and MitoTracker® Red FM were from Invitrogen (Carlsbad, CA). Nunc Lab-Tek II chamber slide system was from Thermo Fisher Scientific (Waltham, MA). 25 nm colloidal gold-labeled anti-mouse IgG was from Aurion (Hatfield, PA).

2.2. Devices

A lambda 25 UV–vis spectrometer (PerkinElmer, Waltham, MA) and a Nicolet 380 FT-IR spectrometer (Thermo Scientific, Waltham, MA) were used for the measurement of absorbance and infrared spectra of C_{60}-polymer complexes. Particle size and size distribution were determined by dynamic light scattering (DLS) using Nano series Zetasizer (Malvern Instruments Inc., Westborough, MA). Atomic force microscopy (AFM) was carried out with MFP-3D microscope (Asylum Research, Santa Barbara, CA) mounted on inverted optical microscope (Olympus, Center Valley, PA). Transmission electron microscopy (TEM) was done with Tecnai GZ Spirit TW device (FEI, Hillsboro, OR) equipped with an AMT digital imaging system (Danvers, MA). Electron paramagnetic resonance (EPR) spectroscopy was performed with a Bruker Biospin e-scan spectrometer (Bruker, Billerica, MA). Confocal microscopy was carried out by LSM 510 Meta Confocal imaging system (Carl Zeiss, Peabody, MA).

2.3. Preparation of C_{60}-polymer complexes

The aqueous dispersions of C_{60}-polymer complexes were prepared by a thin film hydration method with minor modifications [17,25]. Briefly, 1 ml of fullerene in toluene (1 mg/ml) was mixed with 3 ml of PVP or POx in chloroform and stirred at room temperature (r.t.) for 2 h. The C_{60} to polymer molar ratios were varied from 1:0.5 to 1:4. The solvents were removed *in vacuo* at 60 °C to form the thin films. The C_{60}-polymer complexes were readily dispersed in 1 ml of deionized water (DIH_2O), in selected cases using 1–2 min sonication. Excess of unincorporated fullerene was removed by centrifugation (10,000 rpm, 5 min) and filtration through a 0.45 μM filter resulting in a clear yellow colloidal solution. The complexes were dialyzed against water overnight to eliminate the residual toluene and excess of the polymer, and then lyophilized and stored at r.t. for further characterization.

2.4. Characterization of C_{60}-polymer complexes

2.4.1. UV–vis spectroscopy—UV–vis spectra of C_{60}-polymer complexes were recorded and used to determine the concentration of solubilized fullerene by absorbance at 340 nm (the molar absorptivity 49,000 cm l/mol [19]). The fullerene loadings were expressed as %wt. of the dispersed phase (C_{60}-polymer complex dry powder weighted after lyophilization of the dispersions).

2.4.2. Infrared (IR) spectroscopy—IR spectra were recorded using lyophilized powders of free polymers or C_{60}-polymer complexes.

2.4.3. Dynamic light scattering (DLS)—Effective hydrodynamic diameters of the particles were measured by photon correlation spectroscopy (i.e. dynamic light scattering, DLS) in a thermostatic cell at a scattering angle of 90° using the same instrument equipped with a Multi Angle Sizing Option (BI-MAS). Briefly, 0.5 ml of complexes dissolved in DIH_2O at 100 μM C_{60} was used for the measurement. All measurements were performed at 25 °C. Software provided by the manufacturer was used to calculate the size of the particles and polydispersity indices. All the formulations were prepared and measured three times in a parallel manner. The data are presented as means ± SEM. For the stability testing, 0.5 ml of complexes with different pH (pH 2–10), ionic strength (0–1 M NaCl), concentration (1–100 μM) and storage time (1 day–3 weeks at r.t.) were used.

2.4.4. AFM and TEM imaging—For AFM imaging, 10 μl of C_{60}-polymer complexes were dropped on the positive APS mica. The sample was dried under vacuum for 1 h and used for AFM scanning. The data are presented as means ± SEM. For TEM imaging, 10 μl of C_{60}-polymer complexes were dropped at the top of carbon-coated grid. 1% of uranyl acetate solution was applied as the negative staining. The grid was dried for 3 min at r.t. and sent for TEM imaging.

2.4.5. EPR spectroscopy—The ability of C_{60}-polymer complexes to scavenge superoxide was measured by EPR spectroscopy, as we previously reported [37]. Briefly, superoxide generated by HX-XO or a photosensitizer, FMN, was detected using the CMH spin probe. Samples contained 0.025 mM DF and 0.005 mM DETC buffer (pH 7.4), 0.025 mM CMH, 0.025 mM HX and 10 mU XO (or 0.02 mM FMN instead of HX-XO) and C_{60}-polymer complexes at different concentrations. After complete mixing, each sample was incubated at r.t. for 5 min and 50 μl of the sample was loaded into a glass capillary, which was then inserted into the capillary holder of the EPR spectrometer. The CMH radical signal was recorded and EPR spectrum amplitude was quantified.

2.5. Cell culture

CATH.a neuronal cells (ATCC CRL-11179™) were seeded in 6-well plates at 500,000 cells/well or in 24-well plates at 150,000 cells/well (for cytotoxicity studies only) in RPMI-1640 medium (Invitrogen, Carlsbad, CA) supplemented with 1% penicillin/streptomycin, 4% fetal bovine serum (Invitrogen, Carlsbad, CA) and 8% horse serum (Gibco, Life Tech., Grand Island, NY). As previously described [35], CATH.a neurons were cultured at 37 °C with 95% humidity and 5% CO_2, and differentiated by adding 1 mM of fresh N-6,2′-O-dibutyryl adenosine 3′,5′-cyclic-mono-phosphate (AMP, Sigma–Aldrich Co. St-Louis, MO) every 2 days. The cells were typically cultured for 6–8 days for full expression of Ang II receptors on the cell surface. Madin Darby Canine Kidney (MDCK) cells (ATCC, CCL-34), and human liver carcinoma Hep G2 cells (ATCC, HB-8065) were seeded in 96-well plates at 10,000 cells/well in DMEM medium (Invitrogen, Carlsbad, CA) supplemented with 1% penicillin/streptomycin and 10% fetal bovine serum. These cells were cultured at 37°C with 95% humidity and 5% CO_2 for 48 h.

2.6. Cytotoxicity assay

Cytotoxicity of C_{60}-polymer complexes was determined using a cell counting kit (Dojindo Molecular Technologies, Inc., Gaithersburg, MD) according to the protocol provided by the manufacturer. Briefly, cells were seeded in 96-well plates (MDCK, Hep G2) or 24-well plates (CATH.a) and cultured as described above until the media was replaced with the fresh one containing different concentrations of C_{60} complexes. After that the cells were

incubated with the complexes for additional 24 h. The media was then changed for the fresh media containing 10% CCK-8 solution (2-(2-methoxy-4-nitrophenyl)-3-(4-nitrophenyl)-5-(2,4-disulfophenyl)-2H-tetrazolium, monosodium salt). The absorbance at 450 nm was recorded in a plate reader (Molecular Devices, Sunnyvale, CA) after 1 h incubation. The cell viability was calculated as follows:

$$\text{Cell Viability}\,(\%) = \frac{A_{\text{sample}} - A_{\text{blank}}}{A_{\text{control}} - A_{\text{blank}}} \times 100\% \quad (1)$$

Each treatment was repeated three times and data are presented as means ± SEM.

2.7. Cellular uptake in CATH.a neuronal cells

After 6–8 days culture, in 6-well plates CATH.a neuronal cells were exposed to 100 μM of C_{60}-polymer complexes in fresh full medium for 24 h. Then cells were washed twice with 1.0 ml of 0.1 M phosphate buffer (pH 7.4) and lysed with 0.5 ml of 1% triton X-100. The UV–vis spectra of cell lysate supernatant were recorded by a spectrometer. The absorbance was normalized by the cellular protein concentration determined by MicroBCA assay (Pierce, Rockford, IL). The spectrum of the control group (without treatment) was subtracted.

2.8. Immunofluorescence staining and confocal microscopy

The immunofluorescence staining of fullerene has been described elsewhere [15,38]. After 6–8 days culture, CATH.a neuronal cells in chamber slides were incubated with 100 μM C_{60}-polymer complexes in fresh full medium for 24 h. Cells were washed twice with 1.0 ml of 0.1 M phosphate buffer (pH 7.4), stained with MitoTracker® Red FM for 30 min and then fixed with 4% paraformadehyde for 30 min at r.t.. After brief blocking, the fixed cells were incubated with fullerene antibody (1:30 dilution) overnight at 4 °C and then secondary antibody labeled with Alexa Fluor® 488 (1:200 dilution) for 2 h at r.t.. The slides were sealed with coverslips and images were collected using confocal microscopy.

2.9. Immunogold labeling and TEM imaging

The immunogold labeling of fullerene has been described elsewhere [38]. Briefly, CATH.a neuronal cells were exposed to 100 μM of C_{60}-PEtOx complex and cultured as described above. They were then washed twice with 0.1 M phosphate buffer and fixed with 2.5% glutaraldehyde in 0.2 M cacodylate at r.t. for 20 min. Then cells were postfixed in 1% osmium tetroxide in 0.2 M cacodylate for 1 h, dehydrated in ethanol solution and embedded in Agar 100 resin. Thin sections were prepared and incubated with fullerene antibody (1:30 dilution) for 1 h at r.t. and then incubated with 25 nm colloid gold-labeled secondary antibody (1:10 dilution) for 1 h at r.t.. The sections were stained with 1% uranyl acetate and the images were collected using a TEM.

2.10. Intracellular EPR spectroscopy

EPR spectroscopy was used to measure the intracellular superoxide levels in CATH.a neuronal cells, as described before [37]. After 6–8 days culture, CATH.a neuronal cells in 24-well plates were incubated with C_{60}-polymer complexes at different concentrations in fresh full medium for 24 h. Then, cells were washed twice with 0.5 ml of EPR buffer (pH 7.4), and incubated with 1 ml of EPR buffer containing 200 μM of CMH as the intracellular spin probe for 1 h at 37 °C. After incubation ca. 0.9 ml of buffer was aspirated from the well, the cells were scraped from the well and re-suspended with the remaining buffer, and 100 μl of this cell suspension was stimulated with 1 μl of Ang II (100 nM) to generate

intracellular superoxide. Immediately after full mixing, 50 μl of cell suspension were loaded into the EPR spectrometer and the generation of superoxide over 10 min was recorded. The difference in EPR amplitude between the 1st scan (0 min) and 10th scan (10 min) was interpreted as the Ang II-stimulated, superoxide-dependent signal. To control for the difference in cell number between samples, 10 μl of cell suspension were used for cell counting, and the EPR amplitude of each sample was normalized by cell number. Each treatment was repeated three times and data are presented as means ± SEM.

2.11. Statistical analysis

Statistical analysis was done using one-way ANOVA (LSD multiple comparisons). A minimum *p*-value of 0.05 was estimated as the significance level.

3. Results

3.1. Characterization of C_{60}-polymer complexes

We prepared one type of C_{60}-PVP complex (based on PVP 10 kDa) and two types of C_{60}-POx complexes (based on a homopolymer, PEtOx 5 kDa, and a random copolymer, P(EtOx-*co*-BuOx) 8 kDa). The chemical structures of these polymers and the proposed charge-transfer complex formation between fullerene and POx are shown in Fig. 1. The aqueous dispersions of these complexes were optically transparent and revealed the presence of fullerene in the UV–vis spectra, Fig. 2 and Fig. S1 (Supplemental data). For both C_{60}-PVP and C_{60}-POx complexes, similar spectra and specific absorbance of fullerene around 340 nm were recorded. The net amount of solubilized fullerene increased for both C_{60}-PVP and C_{60}-P(EtOx-*co*-BuOx) mixtures as the C_{60}: polymer molar ratio increased from 1:0.5 to 1:4. However, the loading of fullerene practically did not change and varied from 0.6% to about 1% wt. of dispersed phase. Generally, the maximal loading was observed at 1:1 ratio of the components in the initial mixture (Table 1). Interestingly, the solubilization capacity of the more hydrophobic of the two POx, P(EtOx-*co*-BuOx), was comparable to PVP having similar molecular weight, while a more hydrophilic POx, PEtOx, incorporated less fullerene than PVP. Furthermore, the most hydrophilic POx, poly(2-methyl-2-oxazoline) (PMeOx), 5 kDa, was incapable of forming stable dispersions with fullerene (data not shown). These results clearly indicate that the hydrophobicity of POx significantly affects their solubilization capacity for fullerene.

The charge-transfer interaction between PVP and pristine fullerene has been studied before [17]. As shown in Fig. S1, an absorption band at about 430 nm is attributed to the formation of C_{60}-PVP charge-transfer complex. This absorption band was also observed at 430 nm for C_{60}-POxcomplex (Fig. 2b). Chen et al. reported that there is a red-shift for the carbonyl stretching mode of IR spectrum from 1669 cm^{-1} for the free PVP to 1662 cm^{-1} for the complex [39]. This shift indicates that the amide groups of PVP are involved in the charge-transfer interaction between the polymer and fullerene. In the present study, only a minor red-shift of 2 cm^{-1} was found in the IR spectra of C_{60}-POx complex. In these cases the major peak corresponding to the stretching mode of the carbonyl group (amide I band) of PEtOx shifted from 1629 cm^{-1} to 1627 cm^{-1} (Fig. 2c).

The effective size and polydispersity indices (PDI) of the dispersed particles were measured by DLS (Table 1). The representative size distributions of C_{60}-PVP and C_{60}-POx particles are shown in Fig. 3 and Fig. S2. C_{60}-POx complexes formed larger particles (ca. 150 nm and 130 nm for C_{60}-PEtOx and C_{60}-P(EtOx-*co*-BuOx) respectively) compared to C_{60}-PVP complex (ca. 90 nm). For all the polymers used the PDI indices ranged from ca. 0.15 to 0.25. Notably, the particle size and size distribution did not change upon altering pH or ionic strength, and 100-times dilution of the initial dispersion. Furthermore, they did not aggregate

upon storage at r.t. for at least 2 weeks. After this period, aggregation and increase in PDI (to PDI 0.4) was recorded for the C_{60}-PVP complex, while both C_{60}-POx complexes remained stable for an additional week. Despite such remarkable stability in an aqueous dispersion, the fullerene quantitatively recovered and separated from the polymers by extraction into toluene (3:1 v/v).

The representative AFM images are shown in Fig. 3 and Fig. S2. The AFM revealed generally spherical morphology of the particles. In the dry state these particles had mean diameters ranging from 40 nm (C_{60}-PVP) to 96 nm (C_{60}-PEtOx) and mean heights ranging from 5.6 nm (C_{60}-PVP) to 9.7 nm (C_{60}-PEtOx) (Table 2). The spherical morphology was further reinforced by TEM (Fig. 4 and Fig. S3), which also suggested that particles are rather heterogeneous, consistent with both DLS and AFM. TEM further revealed possible inner-structures within some of the C_{60}-PVP and C_{60}-POx particles exhibited as dense formations with relatively high electron density (the dark regions marked by arrows in Fig. 4 and Fig. S3). This may imply that these complexes are composed of one (or more) fullerene-rich domain(s) and a hydrated polymer-rich domain.

3.2. Superoxide scavenging of C_{60}-polymer complexes

The radical scavenging capabilities of antioxidants can be quantitatively evaluated by EPR spectroscopy. In this experiment, superoxide was generated using two different sources: (1) an HX + XO catalytic system or (2) a photosensitizer, FMN. Dose-dependent superoxide scavenging was found in all the formulations tested and was independent of the superoxide source (Fig. 5a and b). The representative EPR spectra are also shown in Fig. 5c–g. Treatment with SOD1, which specifically scavenges superoxide, completely abolished the EPR spectrum (Fig. 5g); thus, corroborating the fidelity of the assay and showing that the CMH radical detected by EPR spectroscopy is superoxide dependent. The C_{60}-PVP and C_{60}-PEtOx complexes exhibited comparable superoxide scavenging activity while C_{60}-P(EtOx-*co*-BuOx) was the least effective. The same scavenging effects as shown for C_{60}-polymer complexes were not observed in the presence of the same concentrations of polymers alone (data not shown).

3.3. Cytotoxicity

The possible toxicity of carbon nanomaterials has been a major concern for their biological applications [40–42]. However, it has been reported that surface functionalization and formulation can efficiently attenuate the toxicity of “naked” fullerene and other carbon nanomaterials such as carbon nanotubes [42,43]. Therefore cytotoxicity of C_{60}-polymer complexes was comprehensively evaluated using three different cell models: MDCK, Hep G2 and CATH.a neuronal cells (Fig. 6). No cytotoxicity was observed upon incubation of MDCK cells with either C_{60}-PVP or C_{60}-P(EtOx-*co*-BuOx) complexes for 24 h (Fig. 6a). However, a minor inhibition of cell growth (80% cell viability) was found in the C_{60}-PEtOx treatment groups at the highest concentration, 100 μM of C_{60}. In Hep G2 cells, C_{60}-PVP and C_{60}-PEtOx exhibited similar toxicity profiles with some toxicity (80% cell viability) at 100 μM of C_{60} (Fig. 6b). Likewise, C_{60}-PVP and C_{60}-PEtOx were not toxic to CATH.a cells up to 50 μM, but decreased cell viability to 80% at 100 μM and were considerably toxic (30% cell viability, $p < 0.01$) at 200 μM (Fig. 6c). Based on these results, C_{60}-PVP and C_{60}-PEtOx complexes were selected for further investigations in the neuron models and the 100 μM was set as the highest concentration in these studies.

3.4. Neuronal cell uptake and distribution

Cellular uptake of C_{60}-PVP and C_{60}-PEtOx into CATH.a neuronal cells was observed, as determined by the UV–vis spectra of cell lysates (Fig. 7a). As shown in Fig. 7a, after 24 h of incubation the lysates displayed specific absorption of fullerene in the vicinity of 340 nm.

Absorption of fullerene in neurons incubated with C_{60}-PEtOx was considerably greater than that of C_{60}-PVP, which suggests that POx-based formulation enhances binding and/or uptake of C_{60} in neuronal cells. The intracellular localization of C_{60} was further examined by immunofluorescence and immunogold labeling (Fig. 7b and c). Consistent with the UV–vis analysis, CATH.a neuronal cells treated with C_{60}-PEtOx exhibited much greater uptake of C_{60}, (green fluorescence) than the C_{60}-PVP-treated neurons (Fig. 7b). No obvious co-localization of fullerene and Mitotracker Red was observed, suggesting that fullerene did not accumulate in the mitochondria after internalization into the cells. The immunogold labeling showed that fullerene was mainly distributed in the cytoplasm and nuclear region (Fig. 7c). No fullerene was found in the mitochondria using this method.

3.5. Intracellular superoxide scavenging

EPR spectroscopy was used to measure intracellular levels of superoxide in Ang II-stimulated CATH.a neuronal cells. As shown in Fig. 8, a significant increase in EPR amplitude, indicating an increase in intracellular superoxide, was detected after 10 min of Ang II stimulation (control vs. control + Ang II, $p < 0.01$). Significant superoxide scavenging was observed upon exposure of cells to C_{60}-PEtOx complex at 100 μM ($p < 0.01$) and 50 μM ($p < 0.05$). Dose-dependent scavenging of intracellular superoxide was clearly evident in this case. Furthermore, 100 μM C_{60}-PEtOx significantly reduced intracellular superoxide levels in CATH.a neuronal cells incubated with another superoxide generator, menadione (Fig. S4). In contrast to C_{60}-PEtOx, C_{60}-PVP did not decrease levels of intracellular superoxide (Fig. 8), which may be due to the limited cellular uptake of this formulation (Fig. 7).

4. Discussion

Free radical scavenging is one promising therapeutic application of fullerene [6,7]. Numerous water-soluble fullerene derivatives have been synthesized and exhibited excellent ROS scavenging capabilities in several disease models. Compared to these functionalized fullerenes, the application of pristine fullerene as ROS scavenger is relatively less explored and hindered by its extreme hydrophobicity. However, due to the ease of manufacturing, low cost, and high yield, it is still worth exploring. Furthermore, some evidence shows that after being properly formulated, pristine fullerene also has a potential as a therapeutic agent for ROS-related diseases and other biomedical applications. For example, the water-soluble C_{60}-PVP complex (Radical Sponge®) has been successfully commercialized by a Japanese company as an antioxidant for skin protection [25]. Recently Misirkic et al. also reported that fullerene formulated with sodium dodecyl sulfate, γ-cyclodextrin or ethylene vinyl acetate–ethylene vinyl versatate copolymer can efficiently protect L929 cells from the cytotoxicity induced by nitric oxide [9]. This study, however, used mechanochemical assisted formulation of C_{60}-based nanoparticles, usually characterized by high PDI, which is a potential impediment for their regulatory approval. Furthermore, the authors suggested that C_{60} might have been chemically modified, presumably due to high shear stress and energy released upon the formulation procedure. Therefore, efficient and biocompatible excipients allowing formulation of fullerene in mild conditions are needed to advance fullerene-based products to a broader clinical use.

During last several years POx have attracted considerable attention in formulation, drug delivery and other biomedical and pharmaceutical applications [44,45]. PMeOx and PEtOx have shown high biocompatibility and similar properties as PEG [46]. However, PEG as a polyether is prone to oxidation and can elicit oxidative stress by itself [47,48]. In the present study, we demonstrated that certain POx can form water-soluble and biocompatible nano-complexes with fullerene. The type of polymer used in such formulations has profound effects on the physicochemical properties of the resulting C_{60}-based nanoparticles, as well

as their intracellular uptake and superoxide scavenging ability. For example, the complex formed by a more hydrophobic POx, P(EtOx-*co*-BuOx), has smaller particle size and lower scavenging activity than those of C_{60}-PEtOx complex. We speculate that P(EtOx-*co*-BuOx) might form dense nanoscale networks around C_{60} molecules (or clusters), which limits the accessibility of superoxide radicals to the fullerene. In contrast, a more hydrophilic PEtOx polymer may form more swollen, bulky, and accessible fullerene-based aggregates.

It has been reported that nanosized aggregates of pristine fullerene cause oxidative damage to the cell membranes and are substantially more toxic than highly water-soluble C_{60} derivatives [42]. We demonstrate here that when properly formulated with water-soluble polymers, both PVP and POx, fullerene does not exhibit any substantial toxicity in kidney, hepatocyte and neuronal cells in a broad dose range. We posit that hydrophilic polymers used in these formulations can effectively mask fullerene from contact with cell membranes and substantially attenuate its cytotoxicity.

The pathogenesis of Ang II-dependent cardiovascular diseases, including hypertension and heart failure, involves an increase in intracellular ROS produced by NADPH oxidases and/or mitochondria [35]. Recent evidence has shown that fullerene has the potential to be used as a scavenger of Ang II-induced ROS in the disease conditions. For example, Maeda et al. reported that a water-soluble fullerene vesicle alleviated Ang II-induced oxidative stress in endothelial cells [49]. In the present study, C_{60}-PEtOx complex showed a considerable intracellular superoxide scavenging effect in CATH.a neuronal cells stimulated with 100 nM of Ang II. Notably, the previously developed C_{60}-PVP system was not active under the same conditions. We believe that differential neuronal uptake is one major reason for different intracellular ROS scavenging activities of these two complexes. Indeed, the neuronal uptake of C_{60}-PEtOx complex is at least two times greater than that of C_{60}-PVP complex. The exact reason for such differential uptake is not clear at the moment. The microstructures of these complexes may play an important role in the process of neuronal membrane binding and uptake. Another possible reason is that compared to PVP, POx may have more favorable interaction and non-specific binding with cell membranes. Recently we reported that the cellular binding and internalization of a model protein, horseradish peroxidase was significantly increased after this protein was conjugated with POx copolymers [36]. In the present study, the greater uptake of C_{60}-PEtOx complex in neuronal cells reinforces potential significance of such formulations as ROS scavengers.

The analysis of intracellular distribution after 24 h of C_{60}-PEtOx complex incubation with cells by TEM imaging showed that fullerene was distributed in both cytoplasm and nuclear region but not in mitochondria. Similar localization was previously found in skin keratinocytes treated with C_{60}-liposome complex [15]. It is worth mentioning that the distribution of POx-based fullerene complexes may be drastically different from that of some water-soluble fullerene derivatives. For example, carboxylated fullerene was localized into mitochondria and inhibited mitochondrial ROS formation [38,50]. In our case the lack of mitochondrial localization may suggest that C_{60}-PEtOx complex can efficiently scavenge the ROS stimulated in the cytoplasm but, probably, not in the mitochondria. Indeed, C_{60}-PEtOx efficiently scavenged 60% of superoxide induced by Ang II stimulation, but only 20–30% of superoxide induced by menadione. This may be explained by different mechanisms of action of these two ROS generators. It is well known that Ang II induces the increase of superoxide in both cytoplasm and mitochondria, while menadione generates superoxide via redox cycling in the mitochondrial electron transport chain [31,35,51]. Altogether, our data indicated that POx-based fullerene formulations have promise as stable, biocompatible and efficient superoxide scavengers in neuronal cells.

5. Conclusion

In the present study, a new type of C_{60}-polymer complexes was prepared and characterized by various techniques. Their physicochemical properties, antioxidant activities and cytotoxicity were evaluated and compared. The possible relationships between activities of superoxide scavenging and formulation factors were discussed. Our results show that C_{60}-PEtOx exhibited greater cellular uptake and significant intracellular superoxide scavenging activity in CATH.a neuronal cells, which is not found in C_{60}-PVP complex. Efficient scavenging of intracellular superoxide induced by Ang II stimulation suggests the therapeutic potential of C_{60}-POx complexes in Ang II-related cardiovascular diseases like hypertension and heart failure. It is also worth mentioning that the safety of POx has been validated and the homopolymer PEtOx has been applied as the excipient in cosmetic industry. Therefore this study also highlights possible applications of C_{60}-POx complexes as cosmetic formulations and treatments of other ROS-related human diseases.

Supplementary Material

Refer to Web version on PubMed Central for supplementary material.

Acknowledgments

This study was supported by the Nanomaterials Core Facility of the Nebraska Center of Nanomedicine supported by NIH COBRE grant RR021937 (awarded to A.V.K.). We also gratefully acknowledge the assistances of UNMC Nanoimaging Core Facility and the Core Electron Microscopy Research Facility (CEMRF) in the AFM and TEM experiments and support by the King Abdullah University of Science and Technology (KAUST Award No. KUK-F1-029-32, partial salary support for R.L.).

References

1. Kroto HW, Heath JR, O'Brien SC, Curl RF, Smalley RE. C60: buckminsterfullerene. Nature. 1985; 318(6042):162–3.
2. Kroto HW, Allaf AW, Balm SP. C60: buckminsterfullerene. Chem Rev. 1991; 91(6):1213–35.
3. Bosi S, Da Ros T, Spalluto G, Prato M. Fullerene derivatives: an attractive tool for biological applications. Eur J Med Chem. 2003; 38(11–12):913–23. [PubMed: 14642323]
4. Krusic PJ, Wasserman E, Keizer PN, Morton JR, Preston KF. Radical reactions of C60. Science. 1991; 254(5035):1183–5. [PubMed: 17776407]
5. McEwen CN, McKay RG, Larsen BS. C60 as a radical sponge. J Am Chem Soc. 1992; 114(11): 4412–4.
6. Markovic Z, Trajkovic V. Biomedical potential of the reactive oxygen species generation and quenching by fullerenes (C60). Biomaterials. 2008; 29(26):3561–73. [PubMed: 18534675]
7. Nakamura E, Isobe H. Functionalized fullerenes in water. The first 10 years of their chemistry, biology, and nanoscience. Acc Chem Res. 2003; 36(11):807–15. [PubMed: 14622027]
8. Yin JJ, Lao F, Fu PP, Wamer WG, Zhao Y, Wang PC, et al. The scavenging of reactive oxygen species and the potential for cell protection by functionalized fullerene materials. Biomaterials. 2009; 30(4):611–21. [PubMed: 18986699]
9. Misirkic MS, Todorovic-Markovic BM, Vucicevic LM, Janjetovic KD, Jokanovic VR, Dramicanin MD, et al. The protection of cells from nitric oxide-mediated apoptotic death by mechanochemically synthesized fullerene (C(60)) nanoparticles. Biomaterials. 2009; 30(12):2319–28. [PubMed: 19195698]
10. Lin TS, Dugan LL, Luh TY. EPR studies of free-radical reactions of carboxyfullerenes. Appl Magn Reson. 2001; 20(4):583–4.
11. Dugan LL, Turetsky DM, Du C, Lobner D, Wheeler M, Almli CR, et al. Carboxyfullerenes as neuroprotective agents. Proc Natl Acad Sci U S A. 1997; 94(17):9434–9. [PubMed: 9256500]

12. Wang IC, Tai LA, Lee DD, Kanakamma PP, Shen CKF, Luh T-Y, et al. C60 and water-soluble fullerene derivatives as antioxidants against radical-initiated lipid peroxidation. J Med Chem. 1999; 42(22):4614–20. [PubMed: 10579823]

13. Lamparth I, Hirsch A. Water-soluble malonic acid derivatives of C60 with a defined three-dimensional structure. J Chem Soc Chem Commun. 1994; 14:1727–8.

14. Chiang LY, Wang LY, Swirczewski JW, Soled S, Cameron S. Efficient synthesis of polyhydroxylated fullerene derivatives via hydrolysis of polycyclosulfated precursors. J Org Chem. 1994; 59(14):3960–8.

15. Kato S, Kikuchi R, Aoshima H, Saitoh Y, Miwa N. Defensive effects of fullerene-C60/liposome complex against UVA-induced intracellular reactive oxygen species generation and cell death in human skin keratinocytes HaCaT, associated with intracellular uptake and extracellular excretion of fullerene-C60. J Photochem Photobiol B. 2010; 98(2):144–51. [PubMed: 20060738]

16. Andrievsky GV, Kosevich MV, Vovk OM, Shelkovsky VS, Vashchenko LA. On the production of an aqueous colloidal solution of fullerenes. J Chem Soc Chem Commun. 1995; 12:1281–2.

17. Ungurenasu C, Airinei A. Highly stable C60/poly(vinylpyrrolidone) charge-transfer complexes afford new predictions for biological applications of underivatized fullerenes. J Med Chem. 2000; 43(16):3186–8. [PubMed: 10956226]

18. Samal S, Geckeler KE. Cyclodextrin-fullerenes: a new class of water-soluble fullerenes. Chem Commun. 2000; 13:1101–2.

19. Yamakoshi YN, Yagami T, Fukuhara K, Sueyoshi S, Miyata N. Solubilization of fullerenes into water with polyvinylpyrrolidone applicable to biological tests. J Chem Soc Chem Commun. 1994; 4:517–8.

20. Shinohara N, Matsumoto K, Endoh S, Maru J, Nakanishi J. In vitro and in vivo genotoxicity tests on fullerene C60 nanoparticles. Toxicol Lett. 2009; 191 (2–3):289–96. [PubMed: 19772904]

21. Xiao L, Aoshima H, Saitoh Y, Miwa N. The effect of squalane-dissolved fullerene-C60 on adipogenesis-accompanied oxidative stress and macrophage activation in a preadipocyte-monocyte co-culture system. Biomaterials. 2010; 31(23):5976–85. [PubMed: 20488530]

22. Ali SS, Hardt JI, Dugan LL. SOD activity of carboxyfullerenes predicts their neuroprotective efficacy: a structure-activity study. Nanomedicine. 2008; 4 (4):283–94. [PubMed: 18656425]

23. Ali SS, Hardt JI, Quick KL, Kim-Han JS, Erlanger BF, Huang TT, et al. A biologically effective fullerene (C60) derivative with superoxide dismutase mimetic properties. Free Radic Biol Med. 2004; 37(8):1191–202. [PubMed: 15451059]

24. Xiao L, Takada H, Maeda K, Haramoto M, Miwa N. Antioxidant effects of water-soluble fullerene derivatives against ultraviolet ray or peroxylipid through their action of scavenging the reactive oxygen species in human skin keratinocytes. Biomed Pharmacother. 2005; 59(7):351–8. [PubMed: 16087310]

25. Xiao L, Takada H, Gan XH, Miwa N. The water-soluble fullerene derivative ‘Radical Sponge ®’ exerts cytoprotective action against UVA irradiation but not visible-light-catalyzed cytotoxicity in human skin keratinocytes. Bioorg Med Chem Lett. 2006; 16(6):1590–5. [PubMed: 16439118]

26. Lens M. Use of fullerenes in cosmetics. Recent Pat Biotechnol. 2009; 3:118–23. [PubMed: 19519567]

27. Pelicano H, Carney D, Huang P. ROS stress in cancer cells and therapeutic implications. Drug Resist Updat. 2004; 7(2):97–110. [PubMed: 15158766]

28. Mapp PI, Grootveld MC, Blake DR. Hypoxia, oxidative stress and rheumatoid-arthritis. Br Med Bull. 1995; 51(2):419–36. [PubMed: 7552073]

29. Dhalla NS, Temsah RM, Netticadan T. Role of oxidative stress in cardiovascular diseases. J Hypertens. 2000; 18(6):655–73. [PubMed: 10872549]

30. Halliwell B. Reactive oxygen species and the central-nervous-system. J Neurochem. 1992; 59(5): 1609–23. [PubMed: 1402908]

31. Zimmerman MC, Davisson RL. Redox signaling in central neural regulation of cardiovascular function. Prog Biophys Mol Biol. 2004; 84(2–3):125–49. [PubMed: 14769433]

32. Welch WJ. Angiotensin II-dependent superoxide effects on hypertension and vascular dysfunction. Hypertension. 2008; 52(1):51–6. [PubMed: 18474831]

33. Laursen JB, Rajagopalan S, Galis Z, Tarpey M, Freeman BA, Harrison DG. Role of superoxide in angiotensin II-induced but not catecholamine-induced hypertension. Circulation. 1997; 95(3):588–93. [PubMed: 9024144]
34. Zimmerman MC, Sharma RV, Davisson RL. Superoxide mediates angiotensin II-induced influx of extracellular calcium in neural cells. Hypertension. 2005; 45(4):717–23. [PubMed: 15699459]
35. Yin JX, Yang RF, Li S, Renshaw AO, Li YL, Schultz HD, et al. Mitochondria-produced superoxide mediates angiotensin II-induced inhibition of neuronal potassium current. Am J Physiol, Cell Physiol. 2010; 298(4):C857–65. [PubMed: 20089930]
36. Tong J, Luxenhofer R, Yi X, Jordan R, Kabanov AV. Protein modification with amphiphilic block copoly(2-oxazoline)s as a new platform for enhanced cellular delivery. Mol Pharm. 2010; 7(4): 984–92. [PubMed: 20550191]
37. Rosenbaugh EG, Roat JW, Gao L, Yang R-F, Manickam DS, Yin J-X, et al. The attenuation of central angiotensin II-dependent pressor response and intra-neuronal signaling by intracarotid injection of nanoformulated copper/zinc superoxide dismutase. Biomaterials. 2010; 31(19):5218–26. [PubMed: 20378166]
38. Chirico F, Fumelli C, Marconi A, Tinari A, Straface E, Malorni W, et al. Car-boxyfullerenes localize within mitochondria and prevent the UVB-induced intrinsic apoptotic pathway. Exp Dermatol. 2007; 16(5):429–36. [PubMed: 17437486]
39. Yu-Huei C, Khairullin II, Mei-Po S, Lian-Pin H. Electron spin resonance and infrared spectroscopy study of the polyvinylpyrrolidone-C60 composite. Fullerene Sci Techn. 1999; 7(5): 807–23.
40. Nel A, Xia T, Madler L, Li N. Toxic potential of materials at the nanolevel. Science. 2006; 311(5761):622–7. [PubMed: 16456071]
41. Mori T, Takada H, Ito S, Matsubayashi K, Miwa N, Sawaguchi T. Preclinical studies on safety of fullerene upon acute oral administration and evaluation for no mutagenesis. Toxicology. 2006; 225(1):48–54. [PubMed: 16782258]
42. Sayes CM, Fortner JD, Guo W, Lyon D, Boyd AM, Ausman KD, et al. The differential cytotoxicity of water-soluble fullerenes. Nano Lett. 2004; 4(10):1881–7.
43. Sayes CM, Liang F, Hudson JL, Mendez J, Guo W, Beach JM, et al. Functionalization density dependence of single-walled carbon nanotubes cytotoxicity in vitro. Toxicol Lett. 2006; 161(2): 135–42. [PubMed: 16229976]
44. Luxenhofer R, Schulz A, Roques C, Li S, Bronich TK, Batrakova EV, et al. Doubly amphiphilic poly(2-oxazoline)s as high-capacity delivery systems for hydrophobic drugs. Biomaterials. 2010; 31(18):4972–9. [PubMed: 20346493]
45. Hoogenboom R. Poly(2-oxazoline)s: a polymer class with numerous potential applications. Angew Chem Int Ed Engl. 2009; 48(43):7978–94. [PubMed: 19768817]
46. Gaertner FC, Luxenhofer R, Blechert B, Jordan R, Essler M. Synthesis, bio-distribution and excretion of radiolabeled poly(2-alkyl-2-oxazoline)s. J Control Release. 2007; 119(3):291–300. [PubMed: 17451833]
47. Sung H-J, Chandra P, Treiser MD, Liu E, Iovine CP, Moghe PV, et al. Synthetic polymeric substrates as potent pro-oxidant versus anti-oxidant regulators of cytoskeletal remodeling and cell apoptosis. J Cell Physiol. 2009; 218(3):549–57. [PubMed: 19016472]
48. Sung H-J, Luk A, Murthy NS, Liu E, Jois M, Joy A, et al. Poly (ethylene glycol) as a sensitive regulator of cell survival fate on polymeric biomaterials: the interplay of cell adhesion and pro-oxidant signaling mechanisms. Soft Matter. 2010; 6(20):5196–205.
49. Maeda R, Noiri E, Isobe H, Homma T, Tanaka T, Negishi K, et al. A water-soluble fullerene vesicle alleviates angiotensin II-induced oxidative stress in human umbilical venous endothelial cells. Hypertens Res. 2008; 31(1):141–51. [PubMed: 18360029]
50. Foley S, Crowley C, Smaihi M, Bonfils C, Erlanger BF, Seta P, et al. Cellular localisation of a water-soluble fullerene derivative. Biochem Biophys Res Commun. 2002; 294(1):116–9. [PubMed: 12054749]
51. Cadenas E, Davies KJ. Mitochondrial free radical generation, oxidative stress, and aging. Free Radic Biol Med. 2000; 29(3–4):222–30. [PubMed: 11035250]

Appendix

Figures with essential color discrimination. Figs. 2, 3 and 7 are difficult to interpret in black and white. The full color images can be found in the on-line version, at doi:10.1016/j.biomaterials.2011.01. 068.

Appendix. Supplementary material

Supplementary data related to this article can be found online at doi:10.1016/j.biomaterials.2011.01.068.

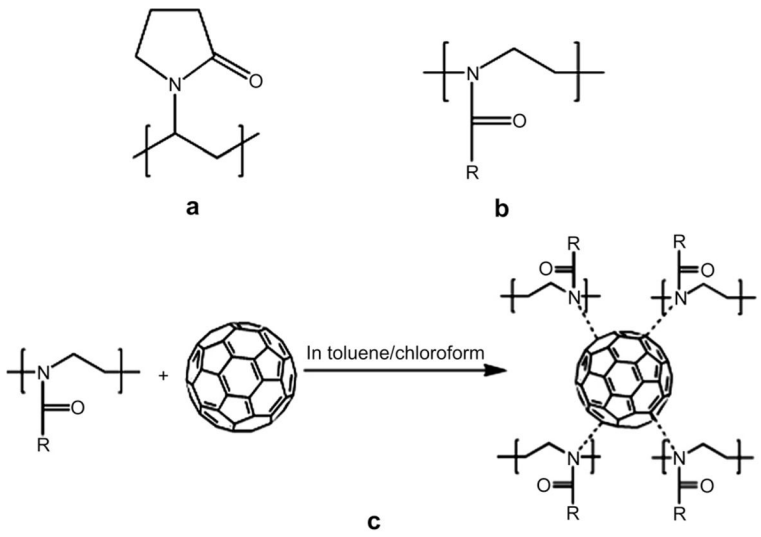

Fig. 1.

Structures of (a) PVP and (b) POx: R = ethyl for PEtOx and R = ethyl or butyl for P(EtOx-*co*-BuOx); and (c) proposed charge-transfer complex formation between fullerene and POx.

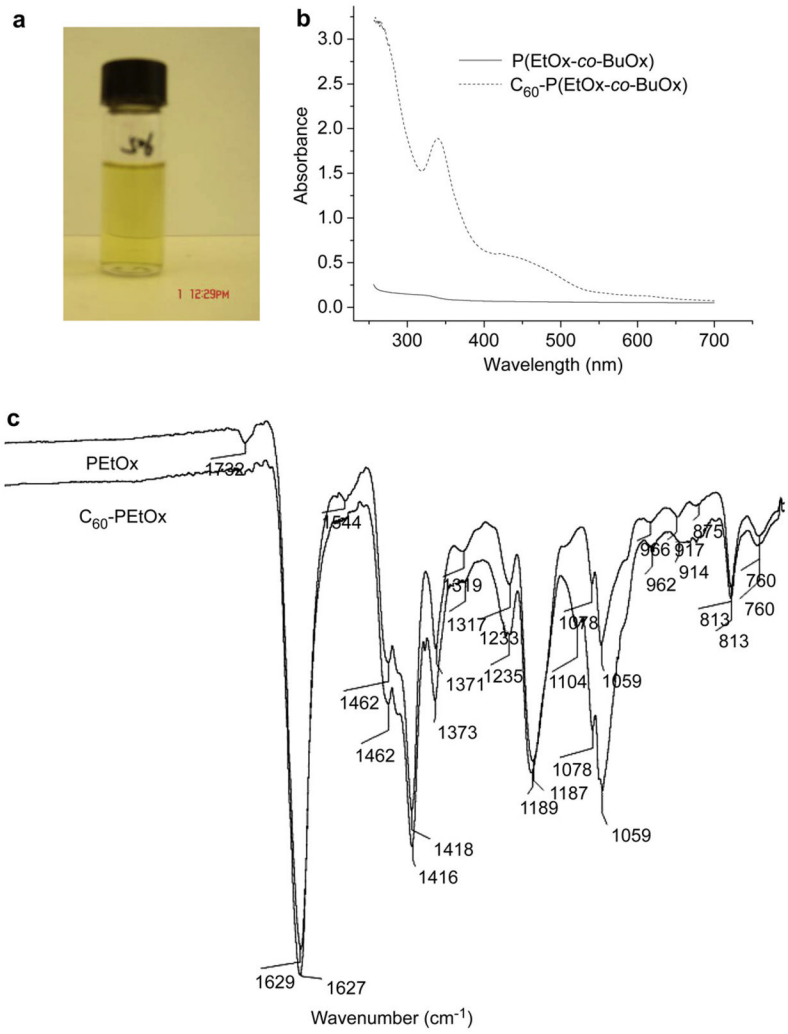

Fig. 2.

Representative C_{60}-POx complexes prepared in the present study: (a) picture of the aqueous dispersion of C_{60}-P(EtOx-*co*-BuOx); (b) UV–vis spectra of P(EtOx-*co*-BuOx) and C_{60}-P(EtOx-*co*-BuOx); (c) Infrared spectra of PEtOx and C_{60}-PEtOx.

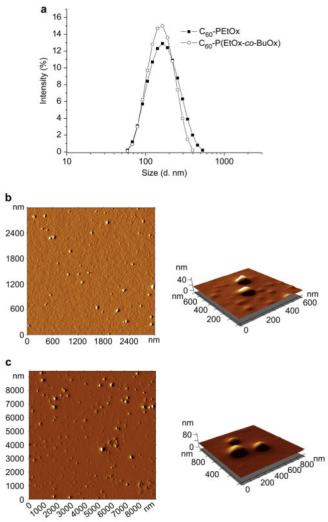

Fig. 3.

Representative size distributions determined by DLS (a) and AFM images (b, c) of C_{60}-POx complexes: (a, b) C_{60}-PEtOx; (a, c) C_{60}-P(EtOx-*co*-BuOx). For AFM, C_{60}-polymer complexes were deposited on the APS mica. Concentration of the complexes is 100 μM in C_{60}.

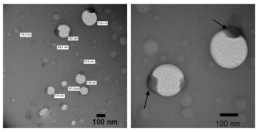

Fig. 4.

Representative TEM images of C_{60}-PEtOx complex obtained with negative staining using 1% of uranyl acetate. Concentration of the complex is 100 μM in C_{60}. The fullerene domains of the complex are marked by arrows.

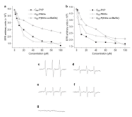

Fig. 5.

Dose-dependent superoxide scavenging by C_{60}-polymer complexes as determined by EPR spectroscopy: (a) 0.025 mM HX and 10 mU XO were used as the superoxide source; (b) 0.02 mM FMN was used as the superoxide source. Representative EPR spectra: (c) HX + XO alone; (d) HX + XO in the presence of 100 μM in C_{60} of C_{60}-PVP; (e) HX + XO in the presence of 40 μM in C_{60} of C_{60}-PEtOx; (f) HX + XO in the presence of 100 μM in C_{60} of C_{60}-P(EtOx-*co*-BuOx); (g) HX + XO in the presence of 400 U/ml SOD1. Each sample was incubated at r.t. for 5 min.

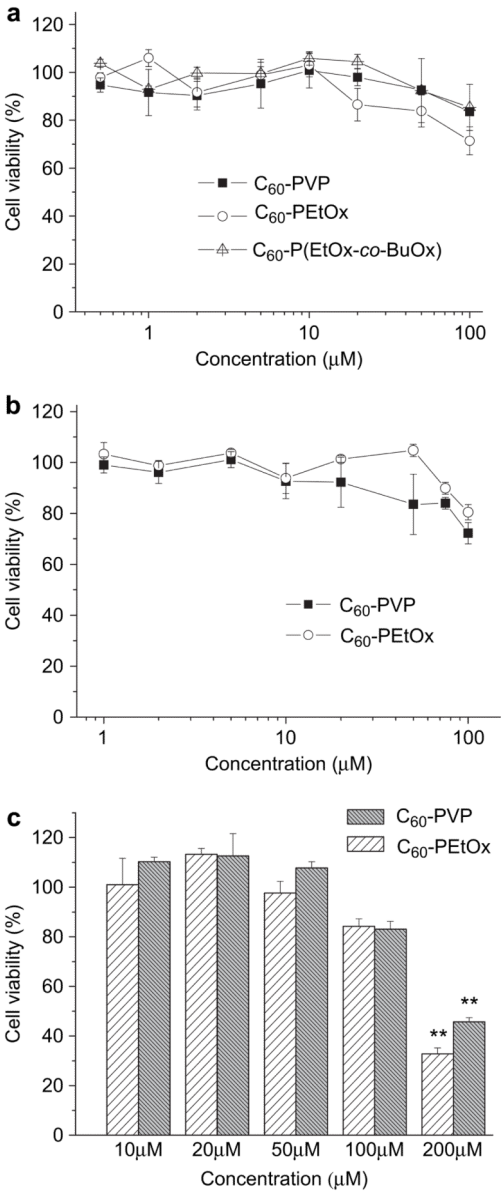

Fig. 6.

Cytotoxicity of C_{60}-polymer complexes in (a) MDCK (b) Hep G2 and (c) CATH.a neuronal cells. Cells were incubated with complexes at different concentrations of C_{60} for 24 h. Cytotoxicity was determined by the cell counting assay. $^{**}p < 0.01$, $n = 3$.

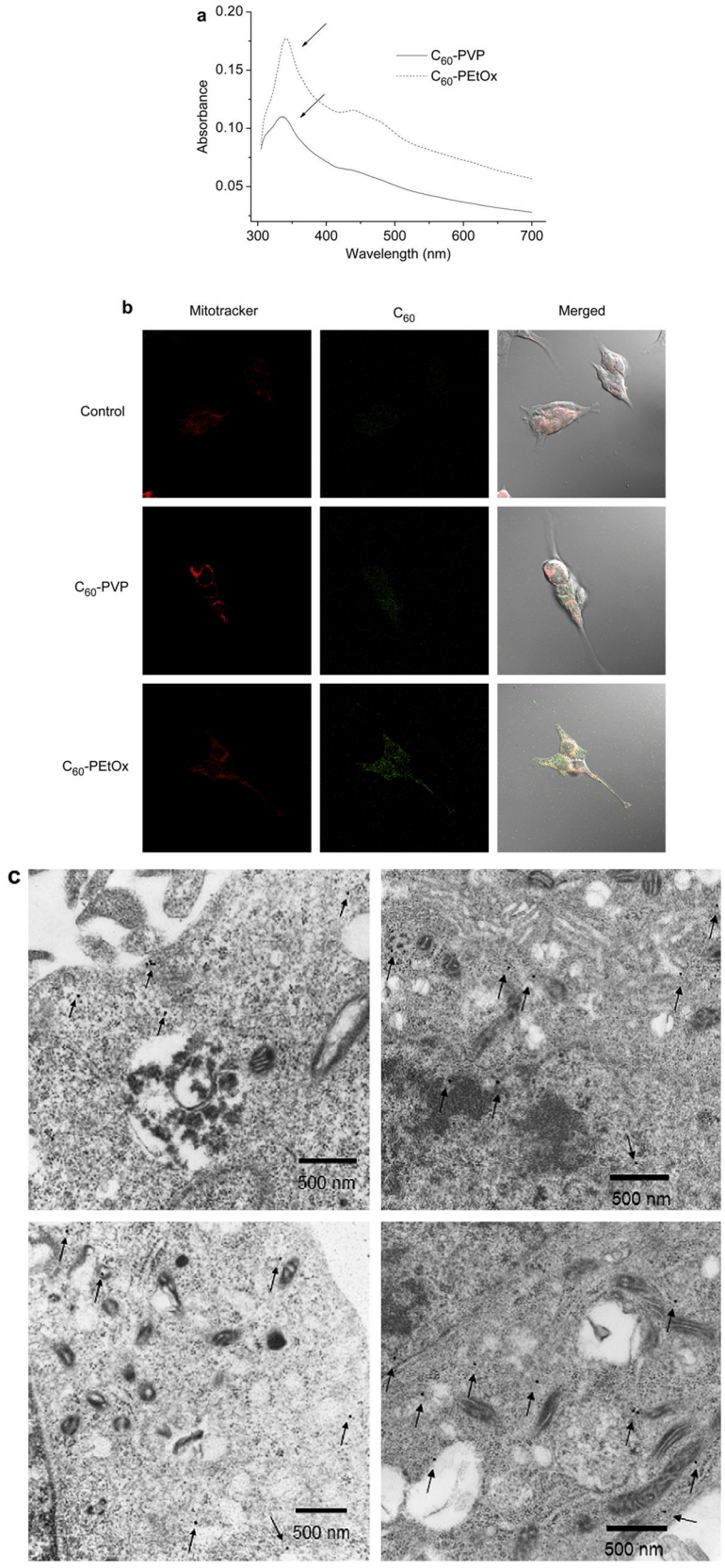

Fig. 7.

Neuronal uptake and sub-cellular distribution of fullerene after 24 h exposure of CATH.a neuronal cells to 100 μM in C_{60} of complexes. (a) UV–vis spectra of supernatant of cell lysates. The absorbance maximum of fullerene at 340 nm is marked by arrows. The absorbance was normalized by the cellular protein concentration determined by MicroBCA assay. The spectrum of the control group was subtracted. (b) Immunofluorescence images of CATH.a neuronal cells treated with C_{60}-PVP or C_{60}-PEtOx complexes. Cells untreated with C_{60}-polymer complexes are shown for comparison. Mitochondria were stained with MitoTracker® Red (red fluorescence). Fullerene was detected with anti-fullerene antibody and then stained with Alexa Fluor® 488 labeled secondary antibody (green fluorescence). (c) TEM images of CATH.a neuronal cells treated with C_{60}-PEtOx complex. Fullerene was detected with anti-fullerene antibody and 25 nm colloidal gold-labeled secondary antibody. The colloidal gold was marked by arrows.

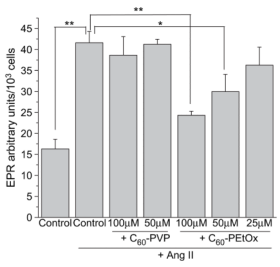

Fig. 8.

Intracellular superoxide scavenging by C_{60}-polymer complexes in CATH.a neuronal cells. CATH.a neurons were treated with various concentrations of C_{60}-PVP or C_{60}-PEtOx complexes for 24 h. 200 μM of CMH was added as the cell-permeable spin probe. Superoxide was generated by stimulating neurons with 100 nM of Ang II. CMH radical signal was recorded by EPR spectroscopy over 10 min. EPR signal was normalized to total cell number. $^{**}p < 0.01$ and $^{*}p < 0.05$, $n = 3$.

Table 1

Characterization of C_{60}-polymer complexes.

Formulations	Particle size (nm)[a]	Polydispersity index (PDI)	Maximal fullerene loading[d] (w/w %)
C_{60}-PVP[b]	94.9 ± 15.21[b]	0.227 ± 0.024	1.0
C_{60}-PEtOx	156.5 ± 22.48[c]	0.217 ± 0.022	0.5
C_{60}-P(EtOx-*co*-BuOx)	132.6 ± 5.94[c]	0.195 ± 0.019	1.0

[a] Particle size and size distribution do not change upon dilution (1−100 μM C_{60}), alteration of pH (pH 2–10) or ionic strength (0–1 M NaCl) of the final dispersion.

[b] For PVP, aggregation is observed after 2 weeks at r.t.

[c] For POx, no aggregation is observed upon storage at r.t. for 3 weeks.

[d] Weight percent of fullerene in dispersion per dispersed phase.

Table 2

AFM characterization of C_{60}-polymer complexes.

Formulation	Mean diameter (nm)	Mean height (nm)	Mean volume (nm^3)
C_{60}-PVP	40.1 ± 1.38	5.6 ± 0.1	9640 ± 356
C_{60}-PEtOx	96.0 ± 3.04	9.7 ± 0.5	49,900 ± 3990
C_{60}-P(EtOx-*co*-BuOx)	57.7 ± 2.77	6.1 ± 0.3	28,800 ± 5750